Journal of Alloys and Compounds 856 (2020) 158057

Contents lists available at ScienceDirect

Journal of Alloys and Compounds

journal homepage: www.elsevier.com/locate/jalcom

Functionalized multi-walled carbon nanotube/polyindole incorporated epoxy: An effective anti-corrosion coating material for mild steel

Saurav Ramesh Nayak[a], Kikkeri Narasimha Shetty Mohana[a,*], Mahesh Bhaskar Hegde[a], Kamalon Rajitha[a], Ambale Murthy Madhusudhana[a], Satishkumar R Naik[b]

[a] Department of Studies in Chemistry, University of Mysore, Manasagangothri, Mysuru, Karnataka 570006, India
[b] Department of Studies in Chemistry, Karnatak University, Dharwad, Karnataka 580003, India

ARTICLE INFO

Article history:
Received 13 August 2020
Received in revised form 16 October 2020
Accepted 20 November 2020
Available online xxxx

Keywords:
Corrosion protection coating
Multi-walled carbon nanotube
Polyindole
Electrochemical impedance spectroscopy

ABSTRACT

The present work destined to enhance the anti-corrosion performance of the epoxy resin (EP) by incorporating the functionalized multi-walled carbon nanotube/polyindole (f-MWCNT/PIn) nanocomposite in the EP matrix. In this direction, the f-MWCNT and f-MWCNT/PIn were prepared, and their chemical compositions were confirmed by Fourier transform infrared (FT-IR) spectroscopy, Raman spectroscopy, X-ray diffraction (XRD), Scanning electron microscopy (SEM), and Transmission electron microscopy (TEM) studies. The corrosion resistance property of different weight percentages of f-MWCNT/PIn dispersed EP coatings on mild steel (MS) in 3.5 wt% NaCl solution was examined by the electrochemical technique. Electrochemical impedance spectroscopy (EIS) and potentiodynamic polarization results indicated that 0.25 wt% f-MWCNT/PIn blended nanocomposite coating exhibits excellent anti-corrosion and barrier protection properties. Uniform dispersion of nanofiller and increasing the pathway of the corrosive electrolytes make it an excellent coating material in anti-corrosion applications.

1. Introduction

Corrosion of carbon steel is the biggest threat to the environment faced by steel structures. It decreases the service life of structures and makes it vulnerable to architectural failures. Therefore, it is essential to monitor and quantify the corrosion behavior and corrosion impact of metal structures to optimize maintenance, improvement, and restoration. General corrosion prevention methods involve coatings on the metal surface such as paints, primers, polymers, and films of various materials, including metal oxides [1]. These films form passive layers which improve the resistance for charge transfer reaction associated with the anodic dissolution of metals and thereby provide protection to metals. The coated layers may be bonded to the metal surface by physisorption or chemisorption [2]. Among several methods, the polymer coating is considered to be the most efficient method to limit the metals to undergo corrosion. However, epoxy/polymer coatings usually applied on the metal surface may suffer failure due to severe environmental conditions. The applied coating can develop corrosion breakdown that begins from the weak areas leading to the formation of blisters, making partial or complete damage to the coated substrate. However, the addition of suitable nanofillers to the epoxy/polymer matrix will enhance the corrosion protection performance of the coatings in terms of stability [3,4].

The carbon-based materials can deliver superior adsorption on the metal surface, hence acts as a corrosion protection barrier in various environments [5]. Carbon nanotubes (CNTs) can be very good nanofillers because of its excellent reinforcing ability for polymer nanocomposites as well as its ultrahigh tensile strength, high thermal and electrical conductivity, and high aspect ratio. The CNTs are said to have the properties of graphite and diamond, and the sp^2 hybridized nature of C-C bonds is accountable for their superior mechanical properties.

Some researchers found that the incorporation of CNTs increases the wear resistance, adhesion strength, and corrosion resistance of the epoxy coatings [6,7]. Jeon et al. [8] studied the corrosion inhibition property of epoxy coating containing multi-walled carbon nanotubes on mild steel. They examined the effect of the MWCNTs on the hydrophobicity and water transport behavior. Cubides et al. [9] reported the influence of zinc content for the protection of carbon steel from corrosion, where the MWCNTs were used as additives in zinc dust pigments. They noticed that zinc-rich pigments display excellent barrier protection during the entire immersion period. Hermas et al. [10] reported the deposition of polyaniline (PANI)–MWCNT composites using *in situ* electro-polymerization on a

* Corresponding Author

https://doi.org/10.1016/j.jallcom.2020.158057
0925-8388/

stainless steel surface and found that MWCNTs decreases the porosity of the PANI. The results also confirmed the formation of the higher resistant passive film on the steel compared to that of pure PANI. Gu et al. [11] studied the effect of the addition of CNT to the polyurethane (PU) on the corrosion of mild steel. They found that the addition of 0.4 wt% CNT into the PU increases the corrosion resistance and adhesion strength of the polyurethane coating. Farag et al. [12] reported the synthesis of PANI/MWCNT composite by oxidative chemical polymerization. They used this composite as a pigment in the resin with different pigment-binder ratios to investigate the anti-corrosive properties of composite coatings on carbon steel in an acid medium. Madan Kumar et al. [13] employed the PANI functionalized MWCNT coating to study the corrosion and mechanical behavior of mild steel (MS) structures. Akbarzadeh et al. [14] reported the fabrication of highly effective PANI grafted CNTs to produce active protective functioning in a silane coating where the role of PANI as a modifier for functionalized CNTs in the silane matrix to deliver active protection to the mild steel. Joshi et al. [15] synthesized the carboxylated MWCNT/polyindole nanocomposite and reported its tremendous potential for electronic applications.

Polyindole (PIn) is a conducting polymer that shows supercapacitor properties when in composite with CNTs [16,17], but its anti-corrosion characteristics are unexplored. In the present work, the carboxy functionalized MWCNT/PIn nanohybrid was dispersed in the epoxy matrix to enhance its anti-corrosion and barrier properties on mild (MS) steel in 3.5 wt% NaCl solution. The electrochemical impedance and potentiodynamic polarization techniques were employed to understand the anti-corrosion behavior of the functionalized MWCNT/PIn nanocomposite coating.

2. Experimental

2.1. Materials and instruments

The multi-walled carbon nanotube (MWCNT), indole (In), and ammonium persulfate were purchased from Sigma Aldrich. All other reagents used were of analytical grade. The Araldite epoxy resin and hardener were purchased from Huntsman Advanced Materials. The MS specimens of measurement 5 cm × 2 cm × 0.3 cm was employed for corrosion studies. The chemical composition of the mild steel sample is given in Table 1.

The synthesized MWCNT/PIn was characterized by Fourier transform infrared (FT-IR) spectroscopy, X-ray diffraction (XRD), Scanning electron microscopy (SEM), Transmission electron microscopy (TEM) and Raman spectral studies. FT-IR spectra were recorded using the Nicolet-5700 FT-IR spectrophotometer. The powder XRD patterns were obtained using the Rigaku miniflex II desktop X-ray diffractometer (Cu-Kα radiation λ = 1.54 Å) with a scan rate of 0.02°/s ranging from 0° to 60°. The Raman spectra were recorded with the PeakSeeker Pro™ Raman system, and the sample stimulated with an inbuilt 785 nm wavelength laser. The contact angle estimations were carried out using the KYOWA interface measurements with an analysis system of FAMAS. TEM analysis was performed using Jeol/JEM 2100, having 200 kV voltage capacity. The electrochemical impedance spectroscopy (EIS) and potentiodynamic polarization measurements were done using an electrochemical workstation, CHI608E, Austin, USA. A conventional three-electrode cell consisting of |Ag/AgCl| as a reference electrode, platinum as a counter electrode, and blank/coated MS sample as a working electrode with 1 cm^2 exposed area.

Table 1
Chemical composition of the mild steel specimen.

Chemical	S	Mn	C	Si	P	Al	Fe
wt%	0.012%	0.13%	0.05%	0.05%	0.010%	0.1%	99.6%

2.2. Functionalization of MWCNTs

The MWCNTs were heated for 1 h at 200 °C, followed by stirring in concentrated HCl for 12 h. The resulting acid-treated MWCNTs was filtered under vacuum and washed thoroughly with distilled water. The functionalization of MWCNTs with –COOH was performed by following the procedure reported by Le [18]. Briefly, 1 g of MWCNTs was immersed in 100 ml of H_2SO_4 /HNO_3 (3:1) and sonicated for 30 min. The solution was then heated for 1 h at 80 °C and filtered under vacuum. The black solid obtained was washed several times with deionized water until the pH of the filtrate became neutral and dried for 12 h at 80 °C under vacuum.

2.3. Synthesis of functionalized MWCNT/polyindole nanocomposite

The indole monomer (2.5 g) was added into 100 ml of 1 M HCl solution and stirred for 30 min. To this, 1 g of functionalized MWCNT (f-MWCNT) was added and continued the stirring for 30 min. To this mixture, ammonium persulfate (0.25 g) dissolved previously in 1 M HCl solution (10 ml) was added drop-wise at 4–5 °C with constant stirring for 1 h [11,19]. The reaction mixture was left overnight at 4–5 °C to undergo polymerization. The resulting f-MWCNT/polyindole (f-MWCNT/PIn) nanocomposite thus precipitated was collected by filtration and dried at 50 °C for 12 h under vacuum. The schematic representation for the preparation of f-MWCNT/PIn is shown in Fig. 1.

3. Results and discussion

3.1. Fourier transform infrared spectral studies

The FT-IR spectra of f-MWCNT and f-MWCNT/PIn are presented in Fig. 2. The oxidation of MWCNT was confirmed by the appearance of peaks at a distinct range for the main functional groups of f-MWCNT. Typical broadband displayed at 3432 cm^{-1}, which characterizes the acidic O–H(O=C–OH) group, and a small peak at

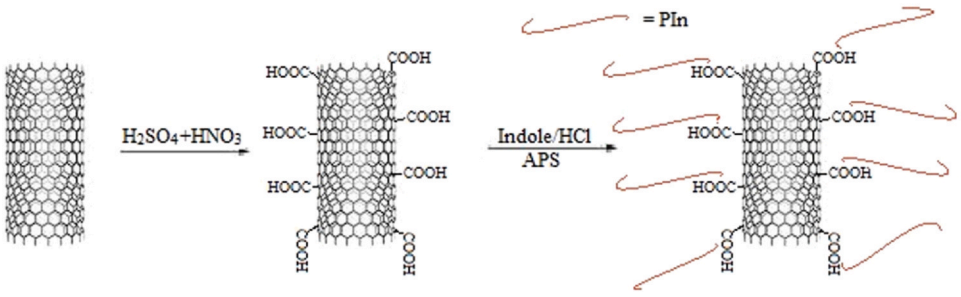

Fig. 1. Schematic representation for preparation of f-MWCNT/PIn nanohybrid.

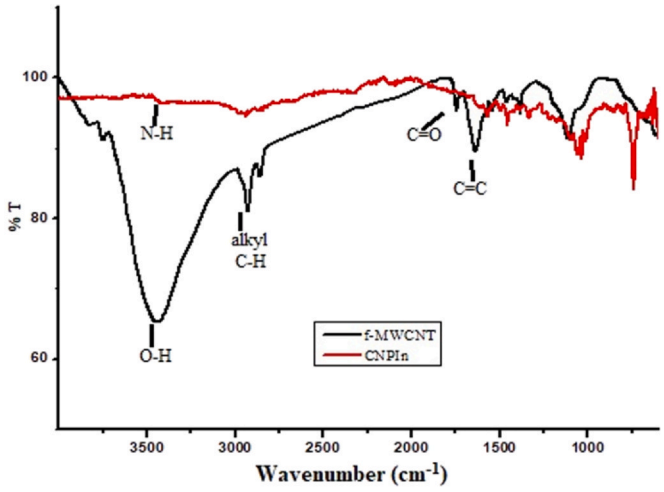

Fig. 2. FTIR spectra of f-MWCNT and f-MWCNT/PIn.

3745 cm^{-1} can be designated to free hydroxyl ions [20]. The two new peaks observed at 1747 cm^{-1} and 1384 cm^{-1} are the evident peaks for C=O (stretch) and C–O (stretch) frequencies, respectively. The peak observed at 2948 cm^{-1} is of alkyl C–H, and a band at 1634 cm^{-1} is displaying the stretching frequency of C=C. These carboxyl and hydroxyl groups on the superficial side of MWCNTs could be due to the oxidation of MWCNT.

In the FT-IR spectrum of f-MWCNT/PIn, a strong peak at 739 cm^{-1} agrees with out of plane bending of the C–H bond of the benzene ring in indole moiety [11,21]. Peaks at 1461 cm^{-1} and 1491 cm^{-1} correspond to the stretching vibration of the benzene ring, which indicates that the benzene ring is not in the polymerization site. Also, bands appeared at 3422 cm^{-1} (N–H stretching) and 1565 cm^{-1} (N–H bending), confirms that the N–H bond is still present. This clearly indicates that the nitrogen present in indole is not in the polymerization site. A medium- weak peak appeared at 1099 cm^{-1} is due to the stretching vibrations of the C–N bond present in indole. The probable site of polymerization in the indole monomer is the 2- and 3-positions. An extensive shift in the peak positions observed in the frequency range of 1000–1600 cm^{-1} is probably due to unlike stretching vibrations of benzene rings [22].

3.2. X-ray diffraction studies

The XRD patterns of MWCNT, f-MWCNT, and f-MWCNT/PIn nanohybrid are shown in Fig. 3. The diffraction peaks of MWCNT are observed at 2θ values of 25.92° and 43.38° [23,24], which are in agreement with the literature results. The first diffraction peak on the left (25.92°) is of very high intensity with less width compared to the second diffraction peak at the right. The f-MWCNT also displays peaks at 26° and 43° with high intensity, along with an additional peak with less intensity at 2θ = 54.22°, which is assigned to the diffraction gap between the walls of MWCNTs and the inter-wall spacing [25]. The XRD pattern of f-MWCNT/PIn showed the characteristic peaks at 19.33° and 26.18°, which are in accordance with both the peaks of PIn and f-MWCNT.

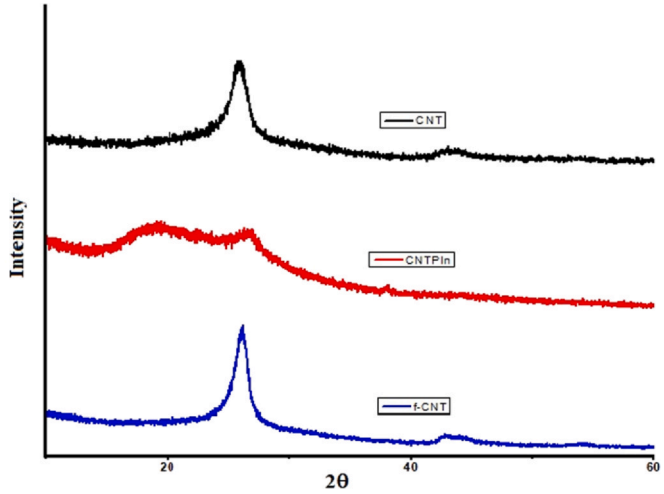

Fig. 3. XRD patterns of MWCNT, f-MWCNT and f-MWCNT/PIn.

3.3. Raman spectral studies

Raman spectroscopy is one of the most convincing methods for studying the structure of carbon-based materials and provides beneficial information on the state of order of the materials and also the state of hybridization of carbon. D band resembles the sp^3 hybridized carbons in the carbon nanotube walls, which generally represents the structural deformation present in the carbon-based materials. The G band assigned to doubly degenerate E_{2g} mode, which indicates the vibrations of sp^2 (double-bonded) carbon atoms in the carbon nanotubes [26]. The Raman spectra of MWCNT, f-MWCNT and f-MWCNT/PIn are displayed in Fig. 4. In MWCNT and f-MWCNT, the D and G bands are observed at 1351 cm^{-1} and 1591 cm^{-1}, which indicates that the oxidation of MWCNTs has not destroyed its graphitic structure since the position of D and G bands are not altered after the oxidation. Whereas in the case of f-MWCNT/Pin, the D and G bands were shifted to 1345 cm^{-1} and 1575 cm^{-1}, respectively. In order to assess efficiently the defects and also the degree of disorder within carbon materials, the I_D/I_G values were

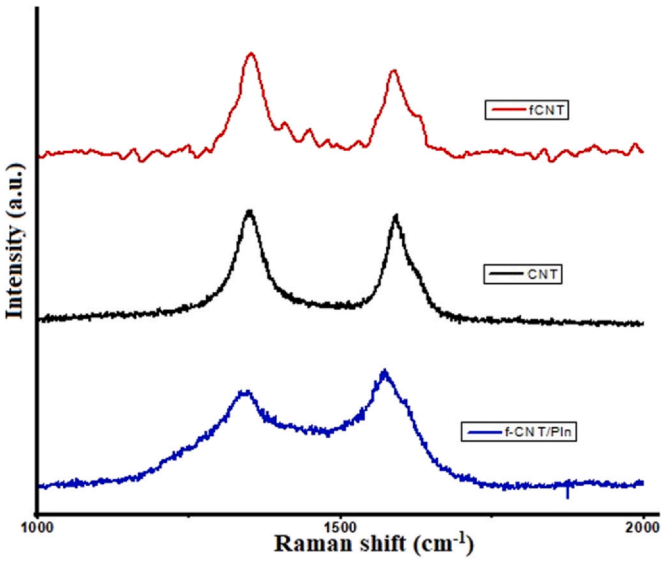

Fig. 4. Raman spectra of MWCNT, f-MWCNT and f-MWCNT/PIn.

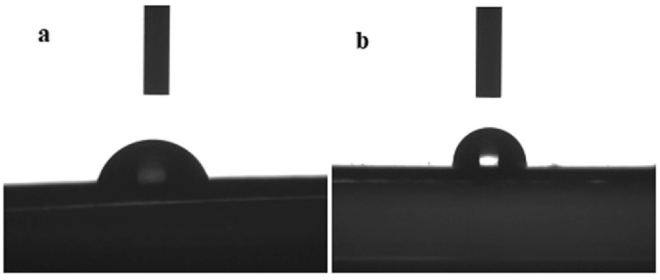

Fig. 5. Contact angle images of f-MWCNT and f-MWCNT/PIn.

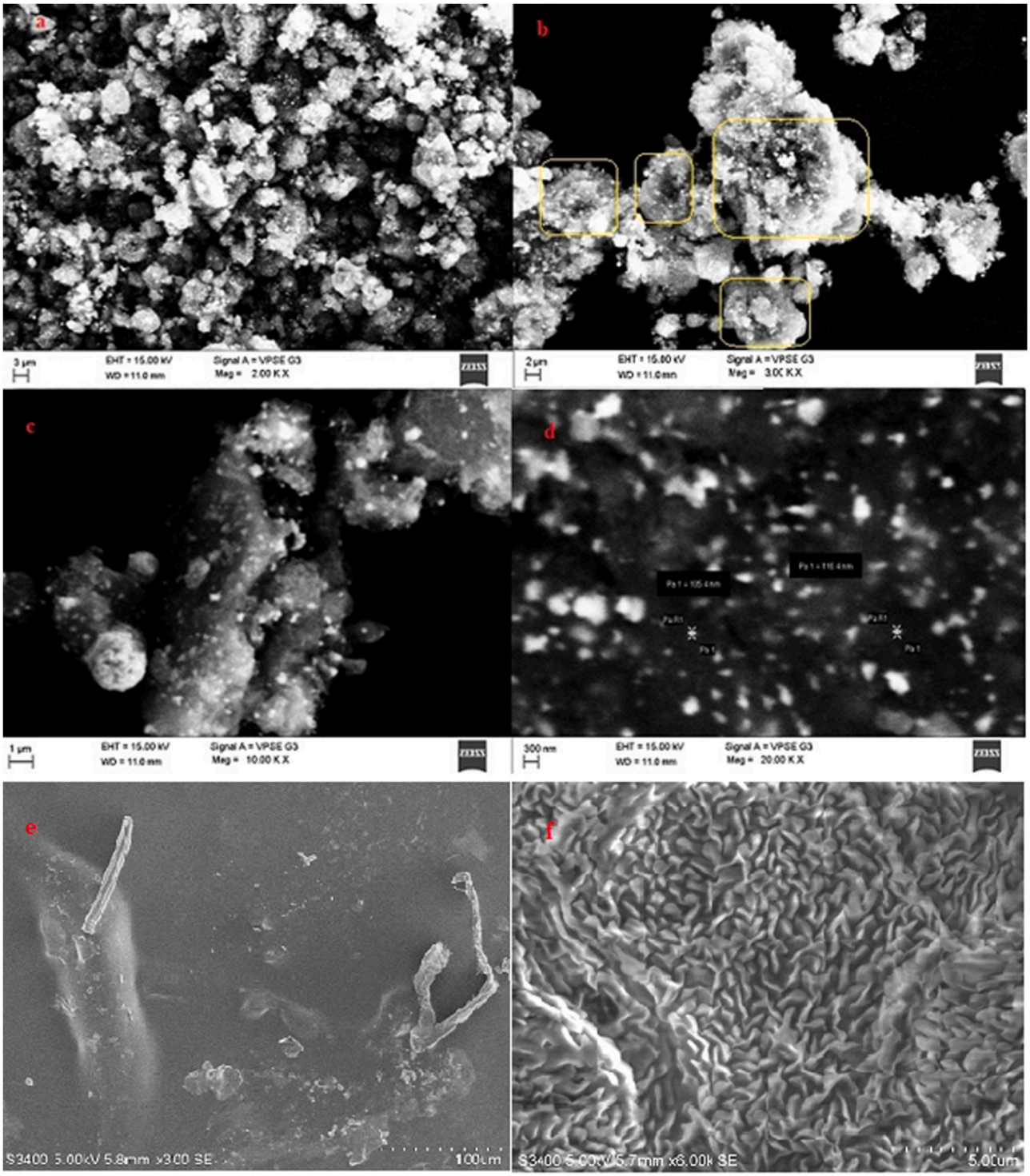

Fig. 6. SEM micrographs of f-MWCNT/PIn.

evaluated, where I represent the intensity of the corresponding peaks. The f-MWCNT showed the highest I_D/I_G ratio (1.103) when compared to that of MWCNT (1.012), which is expected due to the defects formed ($sp^2 \rightarrow sp^3$) during the oxidation of MWCNT [27]. Also, f-MWCNT shows a high value of I_D/I_G ratio than that of f-MWCNT/PIn (0.8045), which suggests that the defect sites on the f-MWCNTs surface might be covered by the polyindole in f-MWCNT/PIn, which causes a decrease in its surface disorder [28].

3.4. Contact angle measurements

Generally, in aqueous environments, coatings having higher hydrophobic nature are typically more repellent to corrosion compared to lesser hydrophobic coatings. Therefore, a correlation among the wettability of a composite coating and its corrosion protective performance is usually required to get complete knowledge about the coating performance in an aggressive environment [15]. The contact

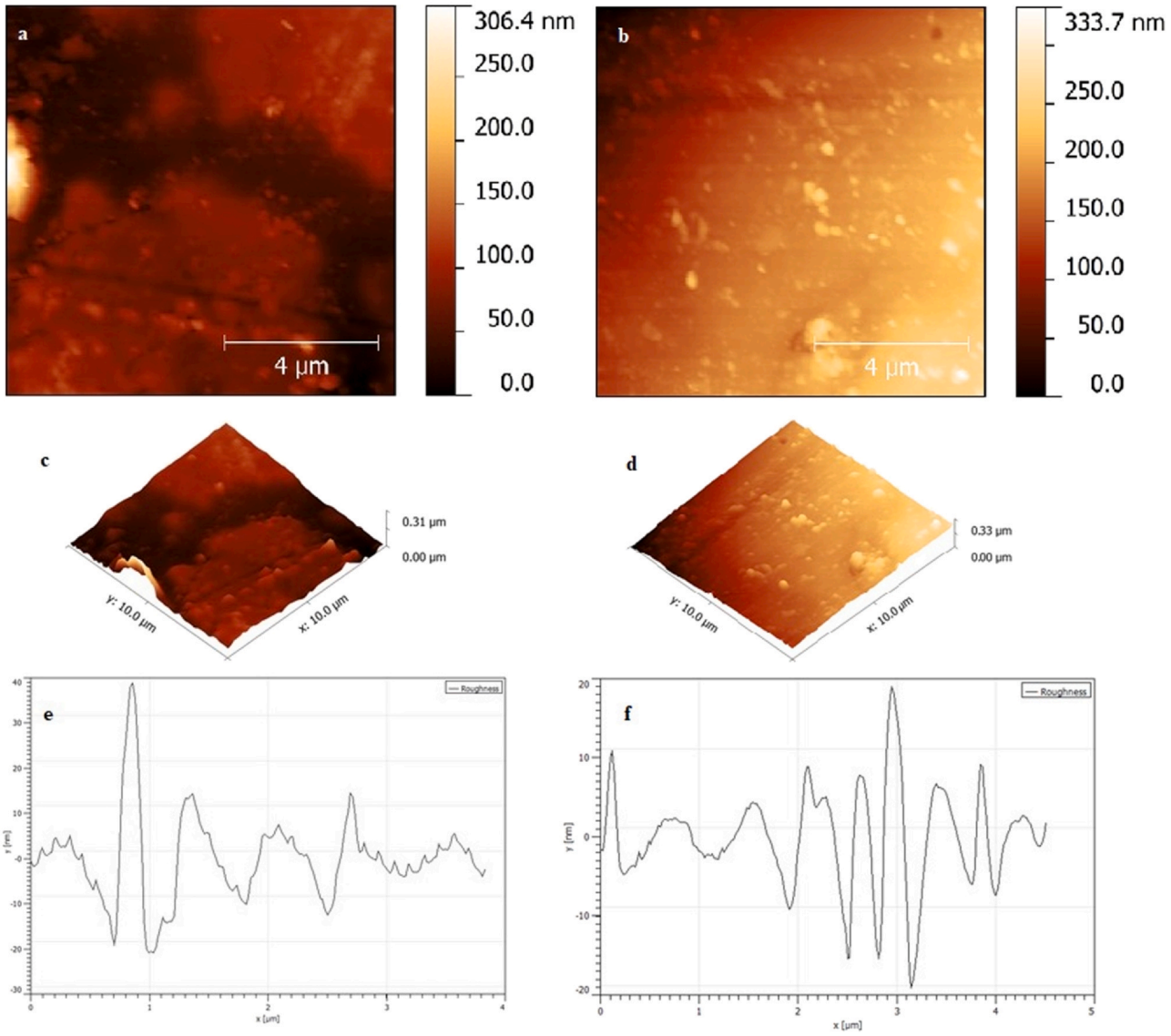

Fig. 7. AFM images of EP and f-MWCNT/PIn coating.

angle analysis was carried out to assess the impact of the modification on the wetting behavior of the coated MS specimens. Fig. 5 shows the water contact angle photographs of epoxy and nanocomposite reinforced epoxy coated MS specimens. The contact angle of the f-MWCNT/PIn dispersed epoxy coated MS specimen was found to be 91°, while the only epoxy coated MS specimen shows 80°, symbolizing the higher hydrophobicity of the nanocomposite coating [29]. The f-MWCNT shows a minor role in increasing the hydrophobicity compared to f-MWCNT/PIn, because of the presence of more number of hydrophilic functional groups on the MWCNTs surface.

3.5. Scanning electron microscopy

Fig. 6 displays the SEM images of as-prepared f-MWCNT/PIn nanohybrid at different magnifications. The Tubular and round-shaped structures were observed in Fig. 6(a). Fig. 6(b) and (c) shows the top and front views of the f-MWCNTs, where Fig. 6(b) displays a thick hollow circular shape of the MWCNT surface covered with PIn (shown in boxes), whereas, the front view of nanohybrid in Fig. 6(c) displays the tube-like structure in which PIn spread along the carbon nanotubes with good adherence [30]. From Fig. 6(d) it can be seen that the diameter of the tube is almost between 105 nm and 115 nm, which is larger than the pristine CNTs. This indicates that the polyindole is coated over MWCNTs during *in situ* polymerization [16]. Fig. 6(e and f) shows the morphology of the well-dispersed f-MWCNT/PIn coated sample.

3.6. Atomic force microscopy

One of the essential factors that affect the adhesion of the coating is surface roughness. AFM images of f-MWCNT/PIn coated surface display the defects present in the coatings such as pinholes and micro-crack. Fig. 7(a and c) and (b and d) shows the 2D and 3D topographical characteristics of EP and f-MWCNT/PIn coatings, respectively, whereas Fig. 7(e and f) displays the roughness of the surface coatings. The estimated values of average roughness (R_a) and root mean square roughness (R_q) of EP and f-MWCNT/PIn coatings are 17.3 nm and 20.5 nm, and 4.5 nm and 6.1 nm, respectively. The decrease in the R_a and R_q on the addition of f-MWCNT/PIn into EP matrix shows that the as-synthesized nanofiller makes the f-MWCNT/PIn nanocomposite superior over the EP coating [31].

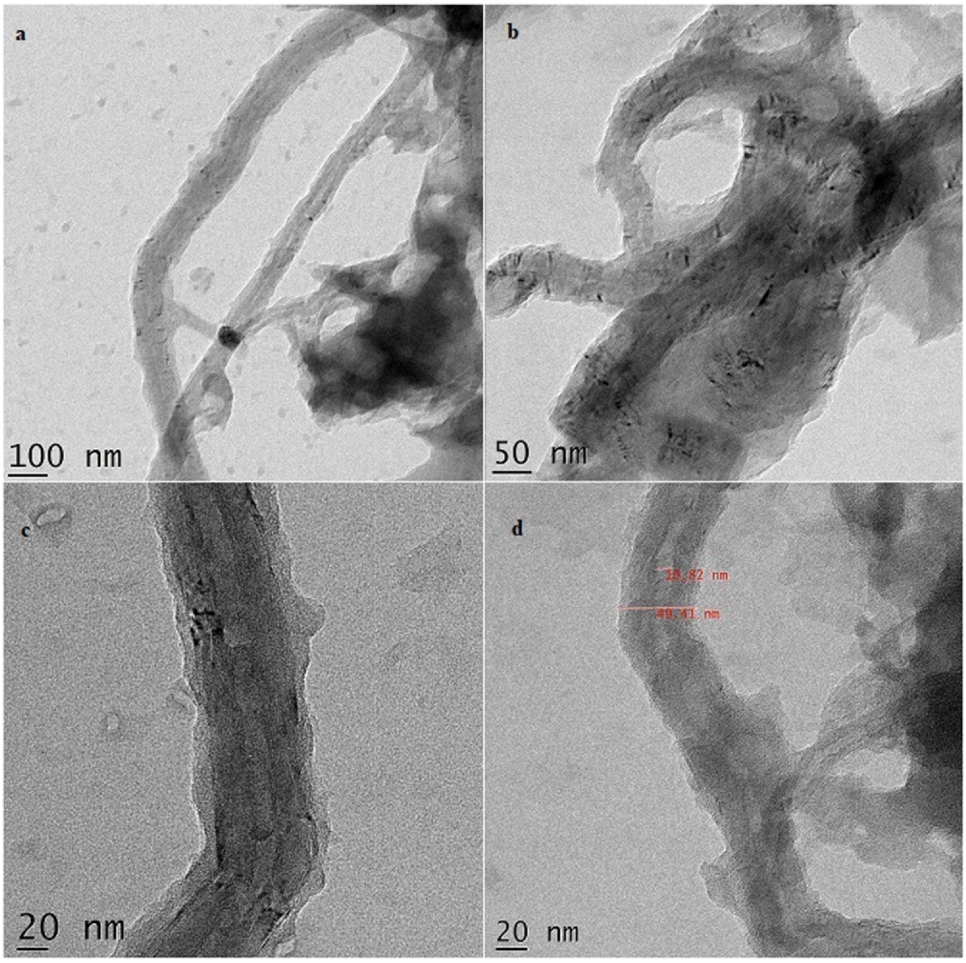

Fig. 8. TEM morphologies of f-MWCNT/PIn.

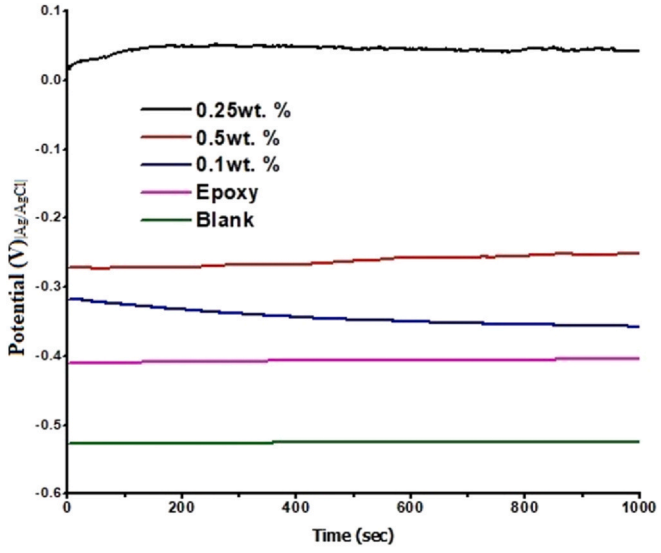

Fig. 9. OCP vs. time plots of blank, epoxy and different wt% of f-MWCNT/PIn nanocomposite coatings in 3.5 wt% NaCl solution.

3.7. Transmission electron microscopy

TEM was used to represent the microstructure and morphologies of f-MWCNT/PIn nanohybrid, which are shown in Fig. 8. Fig. 8(a–c) displays different magnifications of the f-MWCNT/PIn nanohybrid, where PIn covered the surface of the f-MWCNT. Three different layers can be distinguished from the TEM micrograph, in which one is of the inner diameter (hollow) of f-MWCNT, and the second one is the outer diameter of the f-MWCNT, while the last one is the PIn covered f-MWCNT [32]. From Fig. 8(d), it can be seen that the inner diameter of the nanotube is 10.82 nm, while the PIn covered f-MWCNTs is 49.41 nm.

3.8. Corrosion studies

3.8.1. Electrochemical impedance spectroscopy studies

One of the well-known techniques to examine the corrosion resistance of coatings is electrochemical impedance studies. The influence of f-MWCNT/PIn nanofiller in the epoxy matrix was studied to analyze the barrier performance and anti-corrosion property of the epoxy coating on mild steel in 3.5 wt% NaCl solution. The open-circuit potentials (OCPs) of the specimens immersed in 3.5 wt% NaCl solution were recorded before proceeding to EIS analysis. Fig. 9 displays the plot of OCP vs. time during initial immersion. Higher the negative OCP values mean the corrosive electrolytes diffuse into the metal-coating interface [33,34]. From Fig. 9, it can be seen that f-MWCNT/PIn nanofillers incorporated coatings have more positive OCPs compared to that of EP coated and blank MS specimens. Thus it is evident that nanofillers have efficiently prevented the diffusion of corrosive electrolytes. Among the coated samples, 0.25 wt% of f-MWCNT/PIn dispersed nanocomposite coating showed more positive OCP compared to that of 0.5 wt% and 0.1 wt% dispersed coatings. For prolonged immersion, the OCPs of the coatings are observed to

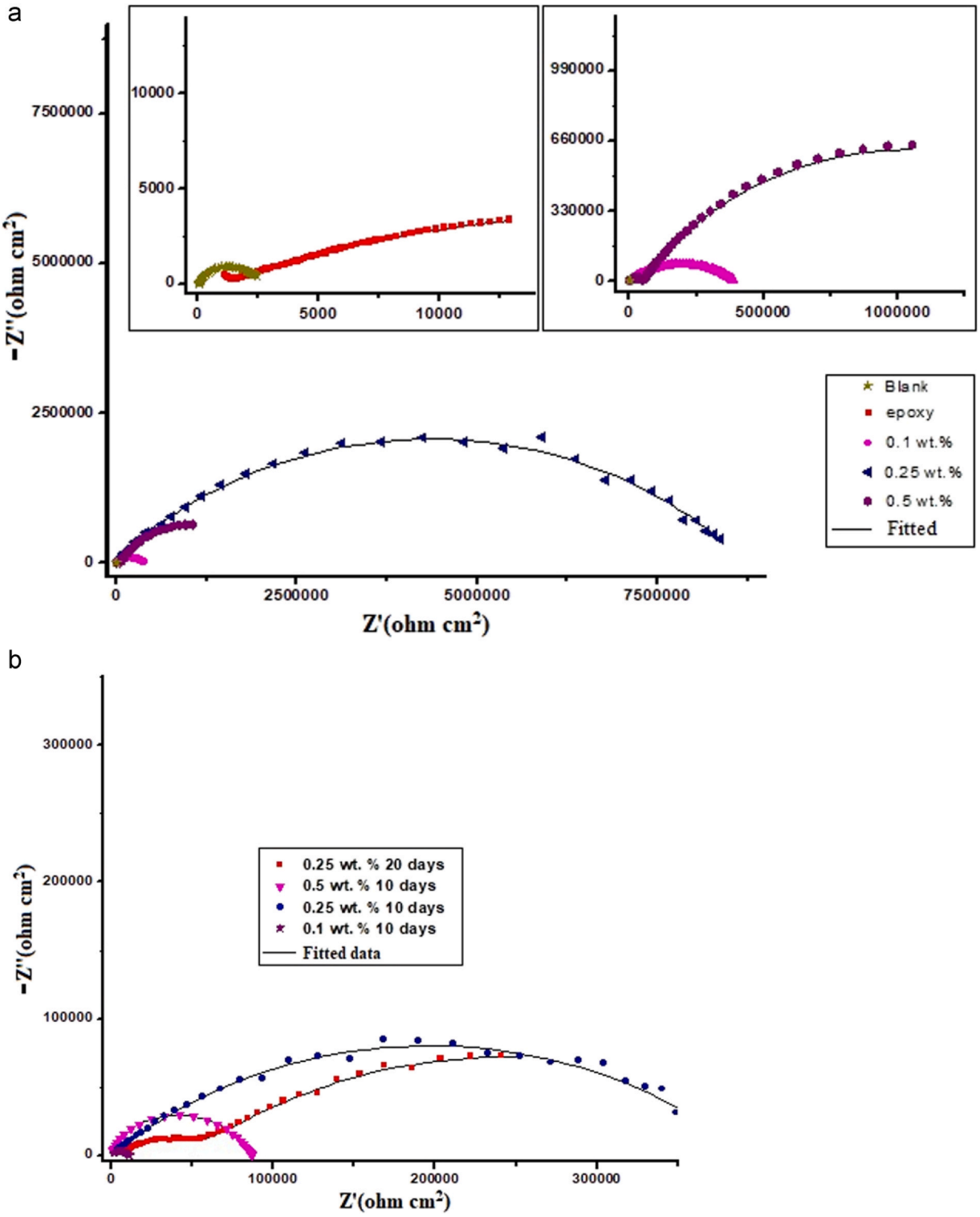

Fig. 10. (a) Nyquist plots of blank, epoxy and different wt% of f-MWCNT/PIn nanocomposite coatings in 3.5 wt% NaCl solution. (b): Nyquist plot of f-MWCNT/PIn nanocomposite coating after 10 and 20 days of immersion in 3.5 wt% NaCl solution.

decrease, indicating the diffusion of corrosive electrolytes through the coatings.

The Electrochemical impedance data of the coated and the uncoated MS specimens are used to examine the anti-corrosion behavior of f-MWCNT/PIn in the EP matrix and are represented in Figs. 10 and 11. Fig. 10(a) and (b) represents the impedance results obtained in the form of Nyquist plots. The tests were carried at room temperature using the bare MS (blank), epoxy coated MS (EP), and different wt% of f-MWCNT/PIn incorporated in EP coated MS in 3.5% NaCl solution. The electrical equivalent circuit was applied to obtain the simulated impedance data [15,35]. The replicated data generated using the equivalent electrical circuits are in good accordance with the experimentally collected data. The obtained circuit is represented in Fig. 12, where R_s is the solution resistance (the resistance between the working and reference electrode), R_c/R_p is the coating resistance (also known as pore resistance), R_{ct} is the charge

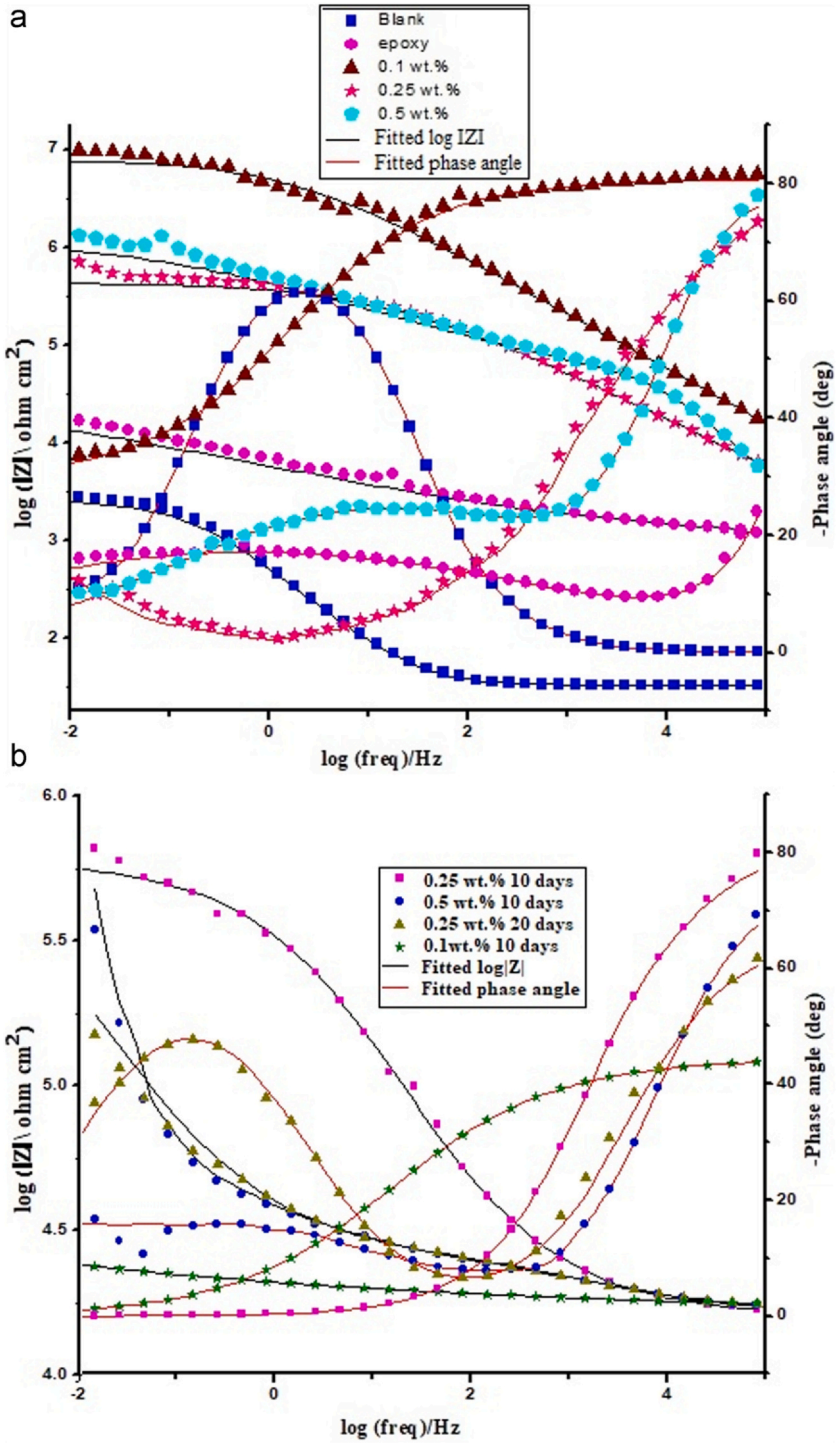

Fig. 11. (a) Bode and phase angle plots of blank, epoxy and different wt% of f-MWCNT/PIn nanocomposite coatings in 3.5 wt% NaCl solution. (b) Bode and phase angle plot of f-MWCNT/PIn nanocomposite coating after 10 and 20 days of immersion in 3.5 wt% NaCl solution.

transfer resistance, Q_c is the constant phase element of the coating, and Q_{dl} is the constant phase element of the double layer.

The impedance of the constant phase element, Z_{CPE}, can be described by the Eq. (1).

$$ZCPE = \frac{1}{Y_o(j\omega)^n} \quad (1)$$

where, Y_o represents constant phase element (CPE) constant, j is imaginary constant and n is CPE exponent (where $0 < n < 1$).

During the first day of immersion, the different wt% of f-MWCNT/PIn incorporated epoxy coatings displayed a semicircle in the Nyquist plot, which has a single capacitance loop. As the diameter of the semicircle is directly related to the corrosion resistance of the coating, 0.25 wt% of f-MWCNT/PIn displays the higher corrosion resistance. The equivalent circuit managed to fit the experimental data comprises of two-time constants, CPE in parallel with its resistance R associated with the hybrid coating [36,37]. R_{ct} refers to the charge transfer resistance of the metal surface, which is inversely proportional to the corrosion rate, and the values of R_{ct} followed the

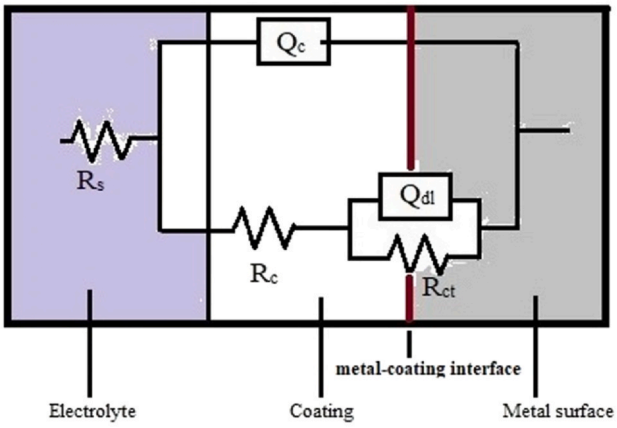

Fig. 12. Fitted equivalent electrical circuit.

same trend as R_c. The diameter of the semicircle in the Nyquist plot of every sample was observed to decrease with increased immersion time. Notably, the composite coatings displayed an increase in the coating and charge transfer resistances compared to EP coated and blank specimens. The presence of f-MWCNT/PIn nanofillers in the coating covers the small pores present in the EP resin by blocking the pathway of corrosive electrolyte to the surface of the MS. Further, it is clear from the results that the incorporation of 0.25 wt% f-MWCNT/PIn into the epoxy caused a significant increase in R_c value.

As the immersion time increases, the corrosive electrolytes start diffusing through the coatings, however, the coating with 0.25 wt% nanofiller shows better corrosion resistance compared to 0.5 wt% and 0.1 wt% dispersed coatings [38]. This is due to the fact that the addition of 0.25 wt% of f-MWCNT/PIn in epoxy forms a good dispersion within the matrix, whereas 0.1 wt% makes it less by leaving a few of the pores unblocked while 0.5 wt% becomes excessive that may end up in the formation of an agglomeration in the coating. Hence the corrosive electrolytes penetrate through the coating quite comfortably in 0.1 wt% compared to 0.5 and 0.25 wt% incorporated nanofillers, respectively.

Fig. 11(a) and (b) represents the Bode plot of the blank and the coated specimens. The corrosion protection abilities of the coatings can be evaluated using logarithmic (log) value of modulus of the impedance at the lowest frequency, i.e., $\log = Z|_{0.01\ Hz}$ and phase angle at the higher frequency, i.e., $\theta_{0.1\ MHz}$. During the initial immersion, only one relaxation time was observed for the coated MS specimens in the Bode phase diagram, which is probably attributed to the fact that the electrochemical results of the coated specimens were essentially under the control of ionic resistance of the coating. The Bode plot illustrates that $\log = Z|_{0.01\ Hz}$ is highest for the 0.25 wt% nanofiller incorporated coating compared to that of 0.5 wt% and 0.1 wt% coatings, which validates the enhancement of corrosion protective resistance of 0.25 wt% coating [39]. The impedance value of 0.25 wt% dispersed nanocomposite coating at low frequency was 10^7 ohm/cm^2 whereas 0.5 wt% and 0.1 wt% were between 10^5 ohm/cm^2 and 10^6 ohm/cm^2, respectively, which shows an increment by nearly more than one order of the $|Z|_{0.01\ Hz}$ for 0.25 wt% coated sample. Similarly, the phase angle at high frequency is another factor for determining the corrosion-resistant behavior of coatings. At an initial immersion of time, the 0.25 wt% nanocomposite dispersed coating has a higher phase angle at high frequency compared to 0.5 wt% and 0.1 wt% incorporated coatings, which are high compared to that of EP coating. The $\theta_{0.1\ MHz}$ of 0.25 wt% of f-MWCNT/PIn added coating was observed at 81° while that of 0.5 wt% and 0.1 wt% were 76° and 73°, respectively. This further confirms that the diffusion of aggressive electrolytes through the coating is tedious, with an increasing pathway in 0.25 wt% f-MWCNT/PIn dispersed in EP [38,40]. During prolonged immersion time, $\log = Z|_{0.01\ Hz}$ and $\theta_{0.1\ MHz}$ of the 0.1 wt% and 0.5 wt% of MWCNT/PIn coatings decreases drastically, whereas 0.25 wt% CPEP coating decreases slightly in 3.5 wt% NaCl solution. From Figs. 10(b) and 11(b), it can be seen that increase in the immersion time causes the reduction in R_c and $|Z|_{0.01}$ values, confirming the continuous diffusion of aggressive electrolytes through the coating [31,41]. The results obtained from the electrochemical impedance spectroscopic studies are noted in Table 2.

3.8.2. Potentiodynamic polarization studies

The polarization curves of the coated and the uncoated MS specimens immersed in a 3.5 wt% NaCl solution are presented in Fig. 13. During initial immersion, all the coated samples shifted towards a positive potential (Fig. 13a), which exhibits that the coating is protecting the MS surface by blocking the pores [42,43]. Generally, lower I_{corr} and higher E_{corr} symbolize better corrosion protection. From the Tafel plot, it is again evident that 0.25 wt% dispersed coating has the highest E_{corr} compared to 0.5 wt%, and 0.1 wt% coatings. Also, I_{corr} of the coatings follows the order. 0.1 wt% > 0.5 wt % > 0.25 wt%. Using the I_{corr} of the coated specimen, the corrosion rate can be computed using the Eq. (2).

$$CR = \frac{kMI_{corr}}{n\rho} \tag{2}$$

where, k is constant, M is the atomic weight of the metal (g/mol), n is the number of charge transfer. The results obtained from the polarization tests are noted in Table 3, in which I_{corr}, E_{corr}, βa, βc, and CR represent corrosion current density, corrosion potential, anodic Tafel slope, cathodic Tafel slope, and the corrosion rate, respectively.

3.9. Corrosion inhibition mechanism

The diffusion of corrosive electrolyte into the metal-coating interface happens because of the small pores/defects presents in the coating or because the delamination of the coatings on metals. This results in the reduction and oxidation reactions happening at the

Table 2
The electrochemical impedance parameters obtained by fitting EIS equivalent circuit for blank, EP and f-MWCNT/PIn incorporated EP coated MS samples in 3.5 wt% NaCl solution.

Sample	R_s	Q_c		R_c	Q_{dl}		R_{ct}
	(Ω cm^2)	Y_o (Ω^{-1} cm^{-2} s^n)	n	(Ω cm^2)	Y_o (Ω^{-1} cm^{-2} s^n)	n	(Ω cm^2)
Blank	2.929×10^1	6.247×10^{-6}	0.39	6.605×10^2	4.396×10^{-5}	0.78	9.417×10^2
EP	1.271×10^2	2.354×10^{-7}	0.64	2.683×10^4	5.221×10^{-7}	0.74	1.087×10^4
0.1 wt% f-MWCNT/PIn	2.786×10^4	2.646×10^{-7}	0.49	3.929×10^6	5.780×10^{-8}	0.00	2.602×10^6
0.25 wt% f-MWCNT/PIn	9.325×10^5	3.079×10^{-9}	0.56	8.717×10^8	2.905×10^{-9}	0.73	2.172×10^7
0.5 wt% f-MWCNT/PIn	6.582×10^4	1.216×10^{-8}	0.73	5.14×10^7	3.428×10^{-8}	0.69	2.061×10^6
0.1 wt% f-MWCNT/PIn (10th day)	2.447×10^2	1.995×10^{-7}	0.59	1.116×10^4	2.954×10^{-6}	0.29	2.844×10^5
0.25 wt% f-MWCNT/Pin (10th day)	4.187×10^5	1.945×10^{-8}	0.86	1.718×10^7	7.909×10^{-8}	0.07	8.334×10^6
0.5 wt% f-MWCNT/Pin (10th day)	1.102×10^4	4.619×10^{-7}	0.65	4.706×10^5	2.365×10^{-8}	0.66	8.681×10^4
0.25 wt% f-MWCNT/Pin (20th day)	3.929×10^3	2.237×10^{-7}	0.50	5.059×10^4	7.162×10^{-6}	0.45	3.752×10^5

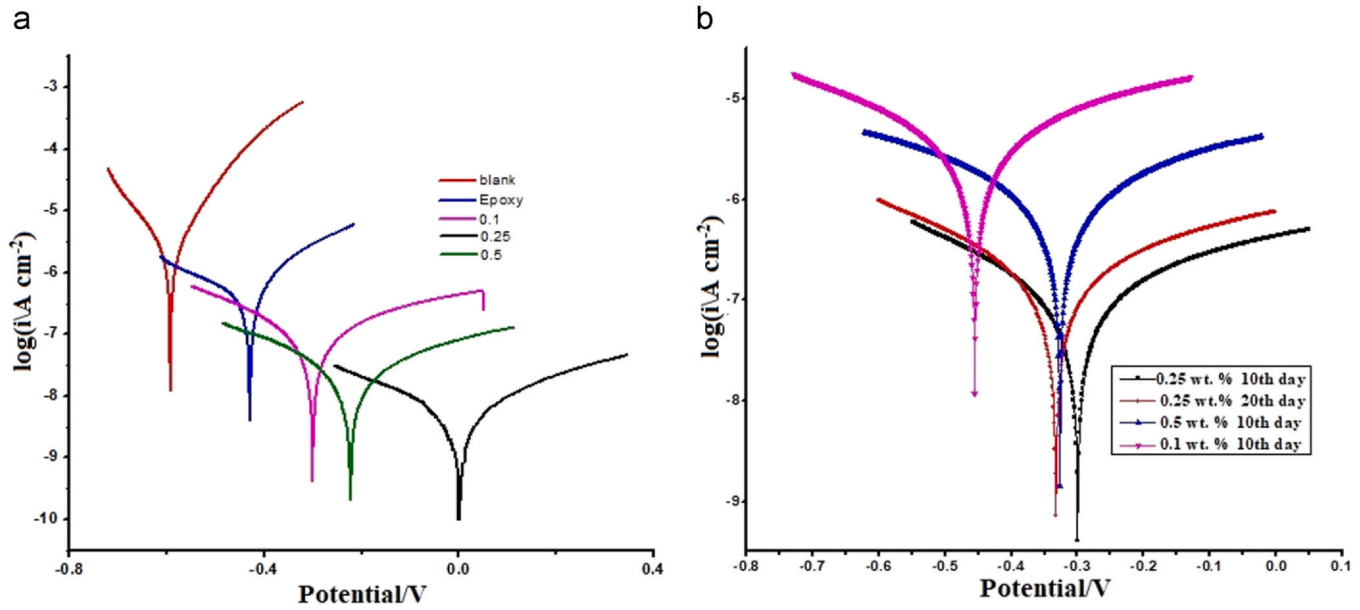

Fig. 13. (a) Tafel plots of blank, epoxy and different wt% of f-MWCNT/PIn nanocomposite coatings in 3.5 wt% NaCl solution. (b) Tafel plots of f-MWCNT/PIn nanocomposite coating after 10 and 20 days of immersion in 3.5 wt% NaCl solution.

Table 3
Potentiodynamic polarization parameters for blank, EP and f-MWCNT/PIn dispersed EP coated MS samples in 3.5 wt% NaCl solution.

Sample	E_{corr} (V)	i_{corr} (A/cm^2)	$-\beta_c$ (V/dec)	β_a (V/dec)	*CR* (Angs/min)
Blank	−0.594	2.328×10^{-6}	10.227	11.406	5.120×10^{-1}
EP	−0.429	7.155×10^{-7}	3.544	5.888	1.573×10^{-1}
0.1 wt% f-MWCNT/PIn	−0.300	7.305×10^{-8}	5.411	4.625	1.589×10^{-2}
0.25 wt% f-MWCNT/PIn	−0.001	4.050×10^{-9}	5.017	5.154	8.905×10^{-4}
0.5 wt% f-MWCNT/PIn	−0.222	1.711×10^{-8}	5.482	4.609	3.763×10^{-3}
0.1 wt% f-MWCNT/Pin (10th day)	-0.456	2.277×10^{-6}	5.126	4.877	5.006×10^{-1}
0.25 wt% f-MWCNT/Pin (10th day)	−0.296	1.826×10^{-8}	4.951	5.040	4.106×10^{-2}
0.5 wt% f-MWCNT/Pin (10th day)	−0.327	6.479×10^{-7}	4.992	4.888	1.425×10^{-1}
0.25 wt% f-MWCNT/Pin (20th day)	−0.333	1.135×10^{-7}	5.335	4.632	4.296×10^{-1}

metal-coating interface, which causes corrosion phenomenon and rust to occur on the metal substrate.

$$Fe \rightarrow Fe^{2+} + 2e^{-} \quad (3)$$

$$O_2 + 2H_2O + 4e^{-} \rightarrow 4OH^{-} \quad (4)$$

Overall reaction is

$$2Fe^{2+} + O_2 + 2H_2O \rightarrow 2Fe(OH)_2 \quad (5)$$

$Fe(OH)_2$ which is also a hydrated ferric oxide ($Fe_2O_3{\cdot}H_2O$), which is rust. From these reactions, understandably, the corrosion of mild steel occurs on reaction with O_2 and H_2O, thus it can be inhibited by preventing O_2 and H_2O from accessing the surface of the metal [44]. So by coating (MWCNT/PIn+EP) composite, MWCNT/PIn blocks the microscopic pores and small defects in the coating [45], which increases the pathway of the electrolyte to reach the coating-metal interface, it is diagrammatically shown in Fig. 14. Thus by controlling the barrier property of the EP coating MWCNT/PIn+EP decreases the possibility of the reduction and oxidation reactions to take place at the interface. This results in less amount of rust and other types of corrosion product formation.

4. Conclusion

The present study explored the role of functionalized MWCNT/PIn (f-MWCNT/PIn) nanocomposite in enhancing the anti-corrosion and barrier properties of EP on mild steel in the saline environment. The carboxy functionalized MWCNT is non-covalently bonded with PIn, and employed as nanofiller in the EP coating. TEM results

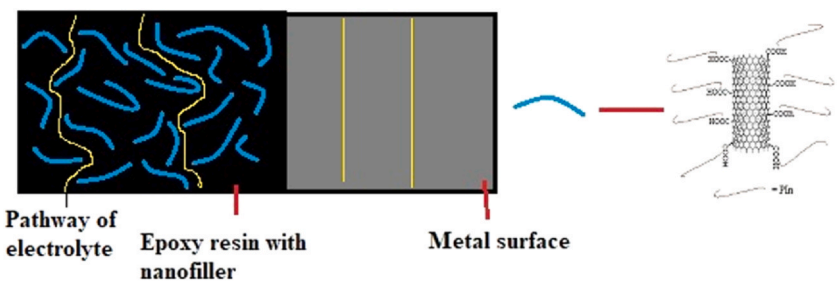

Fig. 14. Schematic representation of the corrosion protection of f-MWCNT/PIn composite coating.

confirmed that f-MWCNT was covered by PIn and is within the nanometer range. The 0.25 wt% f-MWCNT/PIn showed excellent dispersibility in the epoxy matrix compared to 0.1 wt% and 0.5 wt% of nanofillers, and after drying, it showed good hydrophobicity. Electrochemical impedance spectroscopy and potentiodynamic polarization studies showed the excellent barrier protection and anti-corrosion performance in 0.25 wt% of f-MWCNT/PIn coating. The higher corrosion resistance of 0.25 wt% of f-MWCNT/PIn incorporated EP coating may be attributed to its uniform dispersion. Further, the diffusion of aggressive electrolytes through this coating is tedious, with an increasing pathway. Finally, the study concludes that the fabricated nanocomposite is a promising anti-corrosion coating material.

CRediT authorship contribution statement

Saurav R Nayak: Conceptualization, Methodology, Software, Investigation, Formal analysis, Data Curation, Validation, Writing-original draft preparation, Funding acquisition. **Kikkeri N Mohana:** Supervision, Resources, Project administration, Writing - reviewing and editing. **Mahesh B Hegde:** Validation, Investigation, Formal analysis. **Kamalon Rajitha:** Visualization, Data Curation, Formal analysis. **Ambale M Madhusudhana**: Formal analysis, Software, Visualization. **Satishkumar R Naik:** Methodology, Resources.

Declaration of competing interest

The authors declare that they have no known competing financial interests or personal relationships that could have appeared to influence the work reported in this paper.

Acknowledgement

One of the authors, Saurav Ramesh Nayak acknowledges the financial support provided by the University Grants Commission, New Delhi under the scheme UGC-JRF.

References

[1] Y. Qian, Y. Li, S. Jungwirth, N. Seely, Y. Fang, X. Shi, The application of anti-corrosion coating for preserving the value of equipment asset in chloride-laden environments: a review, Int. J. Electrochem. Sci. 10 (2015) 10756–10780.
[2] A. Kühnle, Self-assembly of organic molecules at metal surfaces, Curr. Opin. Colloid Interface Sci. 14 (2) (2009) 157–168.
[3] S. Radhakrishnan, N. Sonawane, C.R. Siju, Epoxy powder coatings containing polyaniline for enhanced corrosion protection, Prog. Org. Coat. 64 (4) (2009) 383–386.
[4] Y. Hayatgheib, B. Ramezanzadeh, P. Kardar, M. Mahdavian, A comparative study on fabrication of a highly effective corrosion protective system based on graphene oxide-polyaniline nanofibers/epoxy composite, Corros. Sci. 133 (2018) 358–373, https://doi.org/10.1016/j.corsci.2018.01.046.
[5] D.H. Xia, S. Song, L. Tao, Z. Qin, Z. Wu, Z. Gao, J. Wang, W. Hu, Y. Behnamian, J.L. Luo, Material degradation assessed by digital image processing: fundamentals, progresses, and challenges, J. Mater. Sci. Technol. 53 (2020) 146–162, https://doi.org/10.1016/j.jmst.2020.04.033.
[6] D. Song, Z. Yin, F. Liu, H. Wan, J. Gao, D. Zhang, X. Li, Effect of carbon nanotubes on the corrosion resistance of water-borne acrylic coatings, Prog. Org. Coat. 110 (2017) 182–186.
[7] N.W. Khun, B.C.R. Troconis, G.S. Frankel, Effects of carbon nanotube content on adhesion strength and wear and corrosion resistance of epoxy composite coatings on AA2024-T3, Prog. Org. Coat. 77 (1) (2014) 72–80.
[8] H. Jeon, J. Park, M. Shon, Corrosion protection by epoxy coating containing multi-walled carbon nanotubes, J. Ind. Eng. Chem. 19 (3) (2013) 849–853.
[9] Y. Cubides, S.S. Su, H. Castaneda, Influence of zinc content and chloride concentration on the corrosion protection performance of zinc-rich epoxy coatings containing carbon nanotubes on carbon steel in simulated concrete pore environments, Corrosion 72 (11) (2016) 1397–1423.
[10] A.-E.A. Hermas, M. Abdel Salam, S.S. Al-Juaid, In-situ electrochemical preparation of multi-walled carbon nanotubes/polyaniline composite on the stainless steel, Prog. Org. Coat. 76 (12) (2013) 1810–1813.
[11] B.E. Gu, C.Y. Huang, T.H. Shen, Y.L. Lee, Effects of multiwall carbon nanotube addition on the corrosion resistance and underwater acoustic absorption properties of polyurethane coatings, Prog. Org. Coat. 121 (2018) 226–235.
[12] A.A. Farag, K.I. Kabel, E.M. Elnaggar, A.G. Al-Gamal, Influence of polyaniline/multiwalled carbon nanotube composites on alkyd coatings against the corrosion of carbon steel alloy, Corros. Rev. 35 (2) (2017) 85–94.
[13] A. Madhan Kumar, Z.M. Gasem, In-situ electrochemical synthesis of polyaniline/f-MWCNT nanocomposite coatings on mild steel for corrosion protection in 3.5% NaCl solution, Prog. Org. Coat. 78 (2015) 387–394.
[14] S. Akbarzadeh, M. Ramezanzadeh, B. Ramezanzadeh, M. Mahdavian, R. Naderi, Fabrication of highly effective polyaniline grafted carbon nanotubes to induce active protective functioning in a silane coating, Ind. Eng. Chem. Res. 58 (44) (2019) 20309–20322, https://doi.org/10.1021/acs.iecr.9b04217.
[15] L. Joshi, A.K. Singh, R. Prakash, Polyindole/ carboxylated-multiwall carbon nanotube composites produced by in-situ and interfacial polymerization, Mater. Chem. Phys. 135 (1) (2012) 80–87.
[16] Z.-J. Cai, Q. Zhang, X.-Y. Song, Improved electrochemical performance of polyindole/carbon nanotubes composite as electrode material for supercapacitors, Electron. Mater. Lett. 12 (6) (2016) 830–840.
[17] H. Mudila, P. Prasher, M. Kumar, A. Kumar, M.G.H. Zaidi, A. Kumar, Critical analysis of polyindole and its composites in supercapacitor application, Mater. Renew. Sustain. Energy 8 (2019) 9.
[18] T.M.H. Le, Characterization of multi-walled carbon nanotubes functionalized by a mixture of HNO3/H2SO4, Diam. Relat. Mater. 89 (2018) 43–51.
[19] R. Oraon, A.D. Adhikari, S.K. Tiwari, S. Bhattacharyya, G. Chandra Nayak, Hierarchical self-assembled nanoclay derived mesoporous CNT/polyindole electrode for supercapacitors, RSC Adv. 6 (69) (2016) 64271–64284.
[20] P. Kar, A. Choudhury, Carboxylic acid functionalized multi-walled carbon nanotube doped polyaniline for chloroform sensors, Sens. Actuators B-Chem. 183 (2013) 25–33.
[21] R.X. Wang, Y.J. Fan, L. Wang, L.N. Wu, S.N. Sun, S.G. Sun, Pt nanocatalysts on a polyindole-functionalized carbon nanotube composite with high performance for methanol electrooxidation, J. Power Sources 287 (2015) 341–348.
[22] T.M. Wu, Y.W. Lin, C.S. Liao, Preparation and characterization of polyaniline/multi-walled carbon nanotube composites, Carbon 43 (2005) 734–740.
[23] S. Liu, J. Yue, R.J. Wehmschulte, Large thick flattened carbon nanotubes, Nano Lett. 2 (12) (2002) 1439–1442.
[24] A. Choudhury, P. Kar, Doping effect of carboxylic acid group functionalized multi-walled carbon nanotube on polyaniline, Compos. Part B- Eng. 42 (6) (2011) 1641–1647.
[25] K.R. Reddy, B.C. Sin, K.S. Ryu, J.C. Kim, H. Chung, Y. Lee, Conducting polymer functionalized multi-walled carbon nanotubes with noble metal nanoparticles: synthesis, morphological characteristics and electrical properties, Synth. Met. 159 (7–8) (2009) 595–603.
[26] K. Huang, J. Zhong, J. Huang, H. Tang, Y. Fan, M. Waqas, B. Yang, W. Chen, J. Yang, Fine platinum nanoparticles supported on polyindole-derived nitrogen-doped carbon nanotubes for efficiently catalyzing methanol electrooxidation, Appl. Surf. Sci. 501 (2020) 144260.
[27] I.S. Zaine, N.A.M. Napiah, A. Mohamad Yusof, A.N. Alias, A.M.M. Ali, S.H. Khalid, Study on dispersion and characterization of functionalized MWCNTs prepared by wet oxidation, Appl. Mech. Mater. 661 (2014) 8–13.
[28] M. Tebyetekerwa, S. Yang, S. Peng, Z. Xu, W. Shao, D. Pan, S. Ramakrishna, M. Zhu, Unveiling polyindole: freestanding As-electrospun polyindole nanofibers and polyindole/carbon nanotubes composites as enhanced electrodes for flexible all-solid-state supercapacitors, Electrochim. Acta 247 (2017) 400–409.
[29] X. Jiang, S. Lou, D. Chen, J. Shen, W. Han, X. Sun, J. Li, L. Wang, Fabrication of polyaniline/graphene oxide composite for graphite felt electrode modification and its performance in the bioelectrochemical system, J. Electroanal. Chem. 744 (2015) 95–100.
[30] X. Zhou, A. Wang, Y. Pan, C. Yu, Y. Zou, Y. Zhou, Q. Chen, S. Wu, Facile synthesis of a Co3O4@carbon nanotubes/polyindole composite and its application in all-solid-state flexible supercapacitors, J. Mater. Chem. A 3 (24) (2015) 13011–13015.
[31] K. Rajitha, K.N.S. Mohana, Application of modified graphene oxide – polycaprolactone nanocomposite coating for corrosion control of mild steel in saline medium, Mater. Chem. Phys. 241 (2020) 122050.
[32] J. Liu, J. Sun, L. Gao, Flexible single-walled carbon nanotubes/polyaniline composite films and their enhanced thermoelectric properties, Nanoscale 3 (9) (2011) 3616.
[33] Y. Cubides, H. Castaneda, Corrosion protection mechanisms of carbon nanotube and zinc-rich epoxy primers on carbon steel in simulated concrete pore solutions in the presence of chloride ions, Corros. Sci. 109 (2016) 145–161.
[34] H. Vakili, B. Ramezanzadeh, R. Amini, The corrosion performance and adhesion properties of the epoxy coating applied on the steel substrates treated by cerium-based conversion coatings, Corros. Sci. 94 (2015) 466–475.
[35] M.B. Hegde, S.R. Nayak, K.N.S. Mohana, N. Kumaraswamy, Garcinia gummigutta vegetable oil–graphene oxide nano-composite: an efficient and eco-friendly material for corrosion prevention of mild steel in saline medium, J. Polym. Environ. 28 (2020) 483–499.
[36] S.R. Nayak, M.B. Hegde, K.N.S. Mohana, Anticorrosion performance of 4- fluoro phenol functionalized graphene oxide nanocomposite coating on mild steel, J. Fluor. Chem. 228 (2019) 109392.
[37] F. Meng, L. Liu, W. Tian, H. Wu, Y. Li, T. Zhang, F. Wang, The influence of the chemically bonded interface between fillers and binder on the failure behaviour of an epoxy coating under marine alternating hydrostatic pressure, Corros. Sci. 101 (2015) 139–154.
[38] S. Pourhashem, M.R. Vaezi, A. Rashidi, M.R. Bagherzadeh, Exploring corrosion protection properties of solvent based epoxy-graphene oxide nanocomposite coatings on mild steel, Corros. Sci. 115 (2017) 78–92.

[39] F. Yu, S. Chen, H. Li, L. Yang, Y. Yin, Application of self assembled 6-aminohexanol layers for corrosion protection of 304 stainless steel surface, Thin Solid Films 520 (15) (2012) 4990–4995, https://doi.org/10.1016/j.tsf.2012.03.006.
[40] B. Ramezanzadeh, S. Niroumandrad, A. Ahmadi, M. Mahdavian, M.H.M. Moghadam, Enhancement of barrier and corrosion protection performance of an epoxy coating through wet transfer of amino functionalized graphene oxide, Corros. Sci. 103 (2016) 283–304.
[41] B. Ramezanzadeh, M.H.M. Moghadam, N. Shohani, M. Mahdavian, Effects of highly crystalline and conductive polyaniline/graphene oxide composites on the corrosion protection performance of a zinc-rich epoxy coating, Chem. Eng. J. 320 (2017) 363–375.
[42] G. Christopher, M.A. Kulandainathan, G. Harichandran, Comparative study of effect of corrosion on mild steel with waterborne polyurethane dispersion containing graphene oxide versus carbon black nanocomposites, Prog. Org. Coat. 89 (2015) 199–211.
[43] M. Ramezanzadeh, B. Ramezanzadeh, M. Mahdavian, G. Bahlakeh, Development of metal-organic framework (MOF) decorated graphene oxide nanoplatforms for anti-corrosion epoxy coatings, Carbon 161 (2020) 231–251, https://doi.org/10.1016/j.carbon.2020.01.082.
[44] A.A. Javidparvar, R. Naderi, B. Ramezanzadeh, Manipulating graphene oxide nanocontainer with benzimidazole and cerium ions: application in epoxy-based nanocomposite for active corrosion protection, Corros. Sci. 165 (2020) 108379, https://doi.org/10.1016/j.corsci.2019.108379.
[45] D.H. Xia, C. Pan, Z. Qin, B. Fan, S. Song, W. Jin, W. Hu, Covalent surface modification of LY12 aluminum alloy surface by self-assembly dodecyl phosphate film towards corrosion protection, Prog. Org. Coat. 143 (2020) 105638, https://doi.org/10.1016/j.porgcoat.2020.105638.